Effect of carbon impurities on the density of states and the stability of hydrogenated amorphous silicon

Thomas Unold,* John Hautala,[†] and J. David Cohen
Department of Physics and Materials Science Institute, University of Oregon, Eugene, Oregon 97403
(Received 22 July 1994)

The effect of trace carbon impurities on the density of states in amorphous silicon has been studied. The deep-defect densities and mobility-gap electronic structure were characterized with electron-spin resonance, drive-level capacitance profiling, and transient photocurrent measurements. Good quantitative agreement in the defect densities deduced from these three methods has been found. This implies a ratio between charged and neutral dangling bonds of at most 2 to 1. Light-induced changes in the mobility-gap electronic structure were also investigated in these films. A small but significant increase in the density of light-induced defects was observed for samples with carbon impurities at the 1 at. % level. The time to saturation of the light-induced degradation for the carbon containing samples was also significantly increased. We discuss the interpretation of these results in terms of two possible mechanisms: either from the presence of carbon-related precursor sites, or by widening of the band gap with carbon alloying.

I. INTRODUCTION

It is well known that impurities can have quite detrimental effects on the electronic properties of crystalline silicon. On the other hand, the role of atmospheric impurities in hydrogenated amorphous silicon (*a*-Si:H) remains controversial, although their effects have been studied for more than a decade. This is particularly true regarding the question of whether light-induced metastable effects in amorphous silicon are related to the presence of such impurities, or whether this phenomenon is of a fundamentally intrinsic nature. Impurity levels for device quality *a*-Si:H films lie in the $10^{17}-10^{19}$-cm^{-3} range for carbon and nitrogen, and in the $10^{18}-10^{20}$-cm^{-3} range for oxygen.[1] Because typical light-induced defect densities in *a*-Si:H are lower than these values, it is conceivable that impurities are involved in the light-induced degradation of amorphous silicon. Indeed, light-induced defect densities in many samples seem to saturate at values around 10^{17} cm^{-3},[2] which has been taken as evidence for a fixed density of precursor sites (e.g., impurities) that are converted into metastable defects.[3]

In general, because the amorphous network is flexible enough to satisfy the valency requirements of a large number of foreign atoms, it is expected that impurities play a considerably smaller role in *a*-Si:H than they do in crystalline silicon. Indeed, such a relative insensitivity to foreign atoms is consistent with the fact that typical *a*-Si:H devices do contain a larger number of impurities than crystalline silicon devices. The higher impurity levels present in *a*-Si:H devices are a result of the [mostly chemical-vapor deposition (CVD)-based] growth techniques which introduce impurities via the contamination of the feed stock gases, outgassing of the chamber, and via hydrocarbons from the oil in the vacuum pumping systems.

Since the first fabrication of devices and solar cells from *a*-Si:H, there have been a number of studies that examined the effect of these impurities on the electronic and optical properties of *a*-Si:H films and device structures. In an early such study Magee and Carlson showed that the addition of impurities such as carbon, nitrogen, and oxygen during growth (at levels below 10^{20} cm^{-3}) significantly reduced the device performance of solar cells, and enhanced the light-induced degradation.[4] Similar results were obtained in other studies of solar cell devices.[5-8] This observed increase in the degradation of contaminated solar cells raised hopes that the light-induced metastable effect could be eliminated altogether if only the impurity content of the material was reduced sufficiently. However, subsequent work revealed that the light-induced degradation did not vanish even when the unintentional impurity levels were sharply reduced by growing films in superclean UHV systems.[9,10] These studies concluded that although there is a measurable effect at higher impurity levels, there is no effect of impurities on the metastable defect density at levels smaller than 5 at. %.

In contrast, we reported several years ago that samples with spatially modulated carbon impurities showed an enhancement of the light-induced degradation at carbon levels below 0.5 at. %.[11] A result consistent with this was obtained in a study by Shimizu *et al.*[12] which reported a small increase in the light-induced defect density for films with a carbon content of 0.8 at. %. The same study found no effect when up to 1 at. % of oxygen or nitrogen was added to the films. Finally, in a more recent study a large number of device-quality films grown by different deposition techniques were characterized electronically and also analyzed for carbon, nitrogen, and oxygen content. In this study, no correlation was found between the saturated metastable defect densities and the impurity content, which lay below 0.2 at. % for all films.[1,13]

To reconcile the disagreement among these studies, one must first recognize that they were performed using

0163-1829/94/50(23)/16985(10)/$06.00 ©1994 The American Physical Society

different characterization techniques and often under quite different experimental conditions. The characterization techniques included were photothermal deflection spectroscopy (PDS), photoconductivity, constant photocurrent method (CPM), electron-spin resonance (ESR), and junction capacitance measurements. The studies usually focused on changes in the total defect densities with varying impurity content, and did not investigate possible changes in the energy distribution of the density of states of the samples. Also, because some of these studies were conducted on devices such as solar cells or Schottky barriers, and others on films deposited on quartz substrates, it has also been suggested that the different results might have arisen because of the different sample configurations used.[13]

In our own earlier study we were able to ensure identical experimental conditions by spatially modulating carbon levels in the samples.[11] However, because of this spatial modulation, it was not possible to obtain corroborating optical absorption or spin signals related to the observed changes in the density of states of these samples. In order to address these issues, we carried out this followup study in which we investigate a series of spatially uniform samples in detail, using a full range of complementary techniques; namely, drive-level capacitance profiling, electron-spin resonance, and transient photocurrent.[14] First of all, this has allowed us to obtain a very complete picture of the change in electron properties with the addition of small levels of carbon impurities $[\mathrm{C}] < 10^{21}$ cm^{-3}. Second, by directly comparing samples with a *p-i*-Schottky barrier geometry and bulk films grown on quartz substrates, we are also able to show that the density of metastable defects does not depend on the different sample geometries, and that the junction-capacitance measurements yield results nearly identical to those obtained by ESR. This level of quantitative agreement between those methods also allows us to set an upper limit on the ratio of charged to neutral dangling bonds, a quantity that has important implications for some models of defect formation.

II. EXPERIMENTAL TECHNIQUES

The samples used in this study were grown in a standard rf-coupled plasma-enhanced chemical-vapor deposition (PECVD) system, with source gases silane and methane diluted in argon.[15] The rf frequency was 13.6 MHz, and the rf power density was 100 mW/cm^2. All samples were roughly 2 μm thick, and were grown simultaneously on heavily boron-doped crystalline silicon wafers and on quartz substrates. The impurity content of the films (carbon, oxygen, nitrogen, and hydrogen) was determined by secondary ion-mass spectroscopy (SIMS) profiling, and exhibited good uniformity ($\pm 5\%$) across the thickness of each sample.[16]

Electron-spin resonance (ESR) measurements were performed at room temperature using a Bruker 300D spectrometer for the samples grown on quartz substrates. Care was taken to avoid microwave saturation, and a background subtraction was made for each measurement. Absolute spin densities were determined by comparing the doubly integrated values with a known spin standard.

Drive-level capacitance profiling (DLCP) measurements[17] were performed on films codeposited on the heavily boron-doped crystalline silicon waves ($\langle 111 \rangle$ orientation) using a thin, semitransparent palladium Schottky barrier on the top of the samples. The DCLP measurements were performed at 360 K and, for consistency, the quartz substrate samples were first annealed at 360 K before each corresponding ESR measurement.

Transient photocurrent measurements were also carried out for the Si wafer substrate films using the same configuration as for the DLCP measurement. The transient photocurrent measurement yields a subband-gap absorptionlike spectrum which can be described by[18]

$$P(E_{\mathrm{opt}}) = K(T,\tau) \int_{E_c - E_{\mathrm{opt}}}^{E_c - E_e} |R|^2 g(E) g(E + E_{\mathrm{opt}}) dE \ , \tag{1}$$

where K is a constant that depends on the measurement temperature T and the time window τ, and where $|R|^2$ is the optical dipole matrix element assumed to be constant in the optical regime studied (0.5–2 eV). Finally, E_e is the thermal emission energy for electrons given by

$$E_e = k_B T \ln(\nu\tau) \ , \tag{2}$$

where ν is the thermal emission prefactor (10^{12}–10^{13} s^{-1}). More details concerning this technique can be found in Ref. 18.

The DLCP method is a junction-capacitance profiling measurement that has proven to be extremely useful for determining the defect density in amorphous silicon alloys.[17,19] Methodologically, it is an extension of the so-called CV-profiling technique which is routinely used to determine the doping level in crystalline semiconductors.[20] In amorphous silicon the density of states is continuous rather than discrete (as in the crystalline case), so that the charge density in depletion is not constant but increases toward the junction interface. Hence, if one were to use the traditional CV profiling technique for the determination of defect densities in amorphous silicon, the results will be strongly skewed by this spatial charge inhomogeneity. It can also be greatly influenced by interface states near the barrier junction.

In contrast, the DLCP method functions to provide a probe of the defect densities within a well-defined spatial region. In addition, it is virtually unaffected by interface states.[17] Defect densities in the DLCP method are determined by measuring the junction-capacitance response C of a sample as a function of the amplitude, δV, of the applied small-signal oscillating component of the applied voltage (at angular frequency ω). Using an expansion of the capacitance

$$C = C_0 + C_1 \delta V + C_2 (\delta V)^2 + \dots \ ,$$

and computing the higher-order coefficients then directly yields the depletion charge density ρ_e near the spatial position where the quasi-Fermi level lies at an energy E_e below E_C:

$$\frac{C_0^3}{2 q_e \varepsilon A^2 C_1} = \frac{\rho_e}{q_e} \ . \tag{3}$$

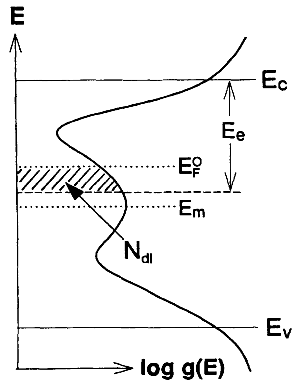

FIG. 1. Schematic showing the portion of the defect band that is detected by the drive-level profiling method (shaded region). The measured value N_{dl} corresponds to the integral of the density of states, $g(E)$, between the neutral bulk Fermi energy E_F^0 and the thermal emission cutoff energy E_e.

The charge density ρ_e is given by an integral over the density of states

$$\frac{\rho_e(x)}{q_e}=\int_{E_C-E_e}^{E_F^0} g(E,x)dE \equiv N_{dl}(E_e,x) . \quad (4)$$

Here E_F^0 is the position of the Fermi energy in the neutral bulk, q_e is the electron charge, ε is the *a*-Si:H dielectric constant, A is the sample area, and the thermal emission depth E_e is given by Eq. (2) with $\omega=1/\tau$.

Thus the DLCP method allows us to profile the energy "slice" N_{dl} of the density of states through the sample. A schematic diagram indicating a typical such "slice" is shown in Fig. 1. The energy range for N_{dl} can be varied either by changing the measurement frequency or temperature. Typical DLCP data obtained on an *a*-Si:H sample for a measurement frequency of 100 Hz, and a series of eight different temperatures are shown in Fig. 2. From Eq. (4) we see that as the thermal emission depth increases with increasing temperature, the value of N_{dl} increases monotonically. However, there must be an upper limit to the value of N_{dl} which is determined by the quasi-Fermi level in deep depletion (as indicated by the energy E_m in Fig. 1). The value of E_m will be given either by the midgap energy position or by the Schottky barrier height (depending on which is largest).[21] Because the Pd Schottky barrier height is approximately 0.9 eV for most of our samples, it is usually possible to profile the density of states down nearly to midgap.

If the dominant deep defect band were centered at midgap, then the total defect density would be obtained by simply doubling the limiting value of the drive-level integral N_{dl}. A better estimate is obtained by noting that, in a series of measurements of N_{dl} vs temperature, there usually exists a well-defined temperature T_{max}, where the rate of increase of N_{dl} with temperature is a maximum. This indicates a peak in the dependence of $g(E)$ vs E_e. For intrinsic *a*-Si:H samples this typically occurs near a temperature of 390 K for a 100-Hz measurement (see Fig. 2; other representative cases can be found in Ref. 19). Thus a good estimate of the total deep defect density is obtained by doubling the value of N_{dl} at T_{max}. To further minimize the effects of thermal annealing during our measurements, we employed a measurement frequency of 10 Hz instead of 100 Hz. This reduces the value of T_{max} to about 360 K. That is, all of the DLCP defect densities reported below will be twice the (spatially averaged) value of N_{dl} obtained at 360 K and 10 Hz.

The samples were light soaked with a Kr ion laser (647 nm) for a variety of exposures, and ranged between 10 and 3×10^4 s, with an intensity of 4.5 W/cm^2 (corresponding to a carrier generation rate of $G\geq4.5\times10^{22}$ cm^{-3}). The corresponding light intensities for the drive-level capacitance and photocurrent samples were adjusted to compensate for the semitransparent Pd contacts.

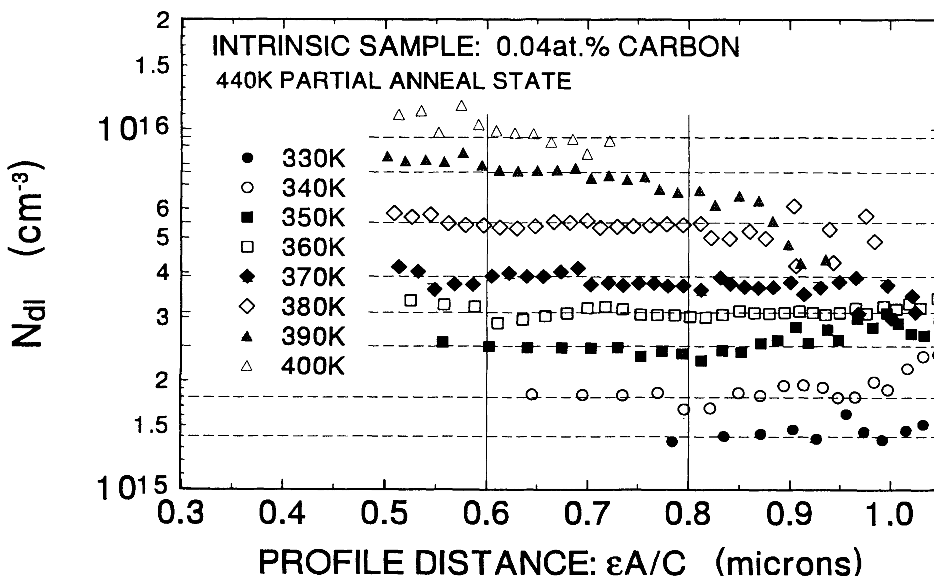

FIG. 2. Example of 100-Hz drive-level profiles for a series of temperatures for one intrinsic *a*-Si:H sample. The dashed lines indicate the spatially averaged value of N_{dl} for the spatial region between 0.6 and 0.8 μm.

The surface temperature of the samples during irradiation was maintained below 65 °C by immersing them in methanol during light soaking.

III. RESULTS

A. Comparison of ESR and drive-level capacitance profiling

In this study we have carried out a systematic comparison of ESR and DLCP measurements on several samples, by determining the defect densities for different light-soaked and annealed states for each sample. As discussed above, the DLCP measurements were performed at low frequencies (10 Hz) and moderate temperatures (360 K) in order to be able to monitor the density of defects down to midgap. (For consistency the corresponding quartz substrate samples were annealed at 360 K before carrying out the ESR measurements.) Our results are shown in Fig. 3, where the DLCP- and ESR-derived defect densities of our most intrinsic amorphous silicon sample are plotted for a wide range of metastable states. As can be seen, the defect densities derived from both measurements are exactly proportional to each other within the accuracy of these methods, even though the defect density itself varies by over a factor of 30. Indeed, within the absolute accuracy of these methods[47] both defect densities are essentially *quantitatively identical.* Figure 3(a) shows the DLCP and ESR results for the series of metastable states obtained for various durations of light exposure, and Fig. 3(b) shows defect densities for different annealed states (following 3×10^4 s of light soaking) of the same amorphous silicon sample. Here the sample was annealed for 30 min at each temperature indicated before the measurement. In all cases we see good agreement between both measurements. The light-induced metastable defects appear to be completely annealed away at a temperature of 490 K.

B. Effect of carbon impurities

Next we compare results for three samples grown with different carbon content. The defect densities as a function of illumination time are shown in Fig. 4(a), as measured by ESR. We see that the spin densities in the annealed state are larger for the samples with higher carbon content, and that this ratio stays approximately constant for all metastable states. Although the defect density of the intrinsic sample clearly shows the onset of saturation, no clear saturation is observed for the samples with higher carbon content even after 9 h of exposure to high-intensity band-gap light. Figure 4(b) shows the same behavior states as measured by the DLCP technique. We again note a difference in the defect densities in the annealed state and in the metastable states, and observe that both ESR and DLCP show the same functional increase in defect densities with light soaking. Again no saturation of the defect densities is apparent for the higher carbon samples, even after light soaking for 3×10^4 s at 4.5 W/cm^2.

In Fig. 5 the transient photocurrent spectra are shown for states A and B (light soaked for 3×10^4 s) of the sample containing 2.6 at. % carbon. We observe that the defect absorption increases by an excitation-energy-dependent factor of up to 30 (at 1.3 eV) between states A and B, which is in good agreement with the values found from DLCP and ESR. In Fig. 6 the transient photocurrent spectra are compared for the light-soaked states (exposure time of 3×10^4 s) of the lowest and highest carbon samples. One notes that in the defect band region of the two spectra, the higher carbon-containing sample exhibits a defect magnitude roughly a factor of 3 higher than the sample with the lowest carbon content. This again is in excellent agreement with the results of the DLCP and ESR measurements. We also note somewhat different spectral shapes for the defect bands in these two samples, indicating different energy distributions for their metastable defects. Finally, in Fig. 7 we compare the transient photocurrent spectra in the dark annealed state of all three samples. Here we note that all spectra exhibit very similar energy distributions in the deep-defect region, but indicate bandtail widths that increase slightly with increasing carbon content. In Table I we have summarized the electronic properties of the samples determined by our measurements.

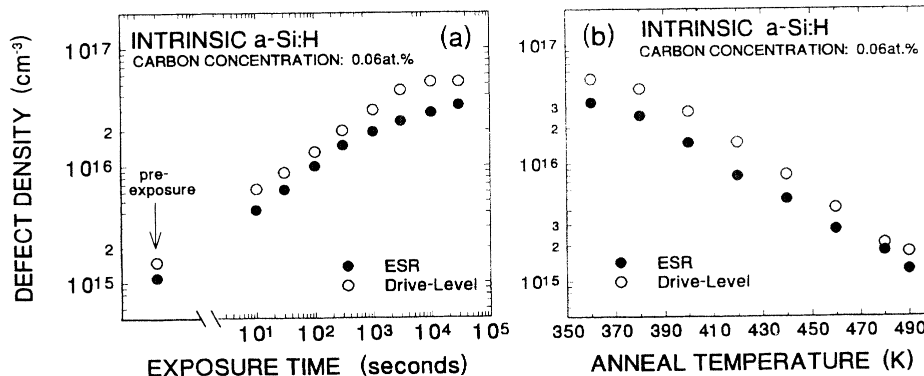

FIG. 3. (a) Comparison of deep-defect densities determined by ESR and drive-level profiling for a series of light-exposed states for an intrinsic *a*-Si:H sample. The drive-level profiles were obtained at 10 Hz and 360 K. (b) Similar comparison for the same sample for a series of partial anneal states following 3×10^4 s of light soaking. The sample was annealed for 30 min at each temperature indicated prior to the ESR and DLCP measurements.

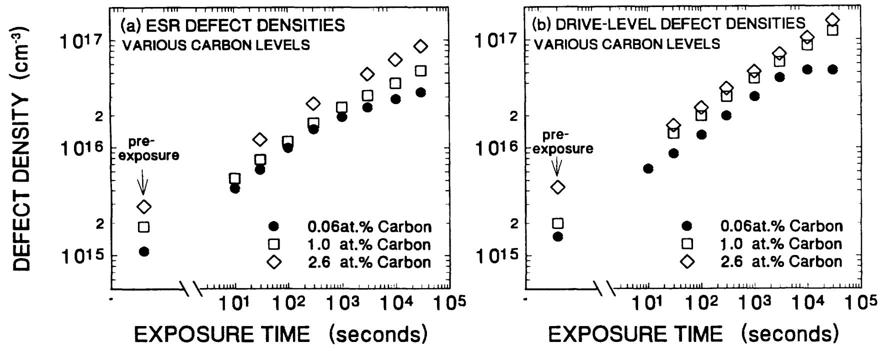

FIG. 4. (a) Comparison of ESR-determined deep-defect densities for three samples containing different levels of carbon impurities as a function of the light exposure time. (b) Same comparison for the deep-defect densities determined by drive-level profiling.

IV. DISCUSSION

A. Comparison of ESR and junction-capacitance measurements

The results of Sec. III established an excellent quantitative agreement between the junction-capacitance and ESR measurements. It was also seen that both measurements gave essentially the same functional behavior for all metastable and partial anneal states. The good quantitative agreement of DLCP and ESR for all light-soaked states also shows that Schottky-barrier samples exhibit the same behavior under light soaking as bulk films grown on quartz substrates.

In the most straightforward interpretation, this quantitative agreement suggests that most of the defects in amorphous silicon are neutral dangling bonds, because the ESR signal detects only unpaired spins, whereas the DLCP technique can detect charged and neutral dangling bonds. However, we note that because of experimental uncertainties in estimating absolute densities our data would also be consistent with equal numbers of negatively charged to neutral dangling bonds. Furthermore, because the DLCP measurement can only detect defects above midgap, it is conceivable that there are more D states located below midgap which can be probed neither by ESR nor DLCP. This would allow the charged dangling bond to neutral dangling bond ratio to exceed unity while still having the DLCP and ESR measurements indicate the same number of defects. However, we believe the ratio cannot be much larger than about 2, or we would see definite evidence of such an excess density of defects below midgap in the optical-absorption spectra. This is *not* observed. Therefore the most plausible interpretation of our data indicates at most similar numbers of neutral and charged dangling bonds. We note that this conclusion contradicts recent suggestions that the ratio may exceed 5 to 1.[22] It is also important to note that the ratio of charged to neutral dangling bonds does not change markedly for our entire series of light-soaked and partial anneal states, again in disagreement with some re-

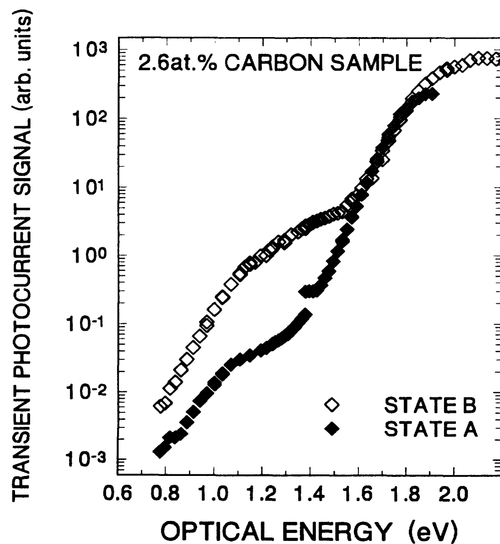

FIG. 5. Comparison of transient photocurrent subband-gap spectra for the 2.6 at. % carbon containing samples before (state A) and after (state B) 3×10^4 s of light soaking.

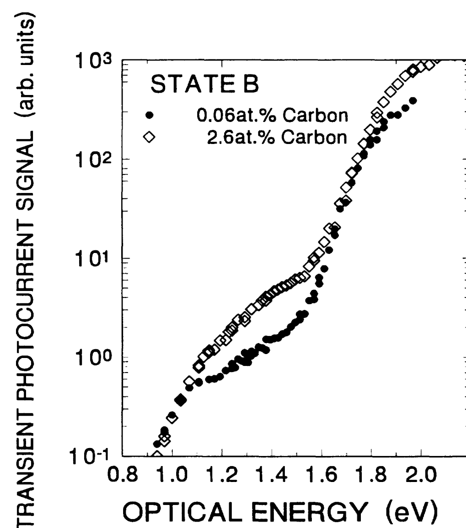

FIG. 6. Comparison of transient photocurrent spectra of the light-soaked states of two samples: one with a 0.06 at. % carbon impurity level, and one with 2.6 at. % carbon. Note the increased defect-related signal for the higher carbon sample, and its distinctly different spectral shape.

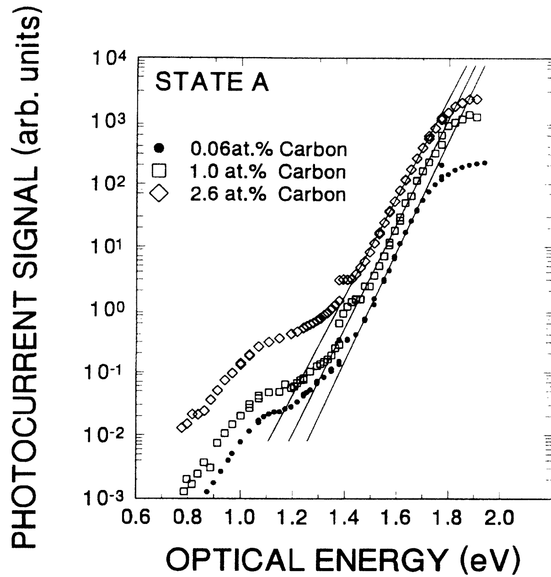

FIG. 7. Comparison of transient photocurrent spectra in the dark annealed state of three samples with different levels of carbon impurities. The spectra have been offset vertically for display purposes. Note the similar shape of the defect-related portion of each spectrum and the increase of the Urbach tail widths as the carbon level is increased.

cent predictions based upon thermodynamical defect creation models.[22] However, this experimental result does not contradict the prediction of defect distributions calculated on the basis of defect relaxation dynamics,[23] since that mechanism predicts a ratio of charged to neutral defects that is independent of the absolute density of defects, provided that the position of the Fermi level is nearly constant.

B. Effect of impurities on the density of states

In Sec. IV A we noted that alloying with carbon produced a small increase in the density of dangling bonds in the annealed state concomitant with an increase in the valence-band tail slope. The slope of the valence-band tail has been generally attributed to the degree of disorder present in a film, such that films with a broader band tails are thought to be more disordered than films with narrower band tails.[24] The valence-band tail states themselves are often considered to be weak silicon-silicon bonds, arising from the strain present in the disordered network. Alloys of amorphous silicon, such as a-Si_xGe_{1-x}:H, a-Si_xN_{1-x}:H, or a-Si_xC_{1-x}:H, are generally found to possess broader band-tail slopes than unalloyed a-Si:H.[25] This is consistent with the idea that alloys tend to induce more disorder and strain in the network, which in turn leads to a larger number of weak bonds. Such effects should indeed be expected if one considers the different bond lengths and bond strengths of silicon, germanium, carbon, and nitrogen.

A larger number of weak bonds present in the network, however, may also result in a larger number of dangling bonds in the material. A direct relationship between the number of weak bonds and dangling bonds in an amorphous network has been given by a simple model proposed by Stutzmann,[26] which has produced good results for amorphous silicon samples, and which also has been recently applied to a-Si_xGe_{1-x}:H alloys with good success.[27]

The idea of the model is that band-tail states (weak bonds) lying beyond a certain demarcation energy E_{db} above the valence-band edge can minimize their energy locally if they form dangling bonds. Hence the number of dangling bonds created during growth is given by the integral over the number of band-tail states which would have been located beyond the demarcation energy E_{db}:[26]

$$N_D=\int_{E_{db}}^{\infty} N_{tail}(E)dE=\int_{E_{db}}^{\infty}[10^{21}\ \mathrm{cm^{-3}\,eV^{-1}}]\exp[-(E-E_V)/E_u)]dE$$
$$=[10^{21}\ \mathrm{cm^{-3}\,eV^{-1}}]E_u\exp\left[\frac{-0.5\ \mathrm{eV}}{E_u}\right], \qquad (5)$$

where we have assumed an exponential valence-band tail with slope E_u, and where we have assumed a value of $E_{db}=0.5$ eV above E_V. To predict the defect densities for our samples from Eq. (5), we assume that a small addition of carbon only changes the Urbach tail slope and not the demarcation energy E_{db}. Figure 8 shows the predicted values and the measured defect densities for our samples, and it can be seen that both agree well within the experimental uncertainty. Thus the increase in the annealed state defect density in samples with larger concentrations of carbon impurities can be attributed to an increase in the number of weak bonds arising from increased disorder, and strain induced by the additional carbon atoms. As mentioned above, such "alloying effects" have also been found in earlier studies of amorphous silicon-germanium alloys, where the Urbach tail slope was often found to increase dramatically with germanium incorporation.[25,28] More recently, however, it has been possible to grow silicon-germanium alloys with valence-band-tail slopes that are essentially fixed at values found for device-quality amorphous silicon.[27,29] This suggests that in these alloys it has been possible to mini-

TABLE I. Comparison of electronic properties for samples with different levels of carbon impurities before and after light soaking. The quantities N_d and N_s denote the defect densities determined by drive-level capacitance profiling and by electron-spin resonance, respectively.

Sample	$[C]$ ($\mathrm{cm^{-3}}$)	E_u (meV)	$N_s(A)$ ($\mathrm{cm^{-3}}$)	$N_d(A)$ ($\mathrm{cm^{-3}}$)	$N_s(B)$ ($\mathrm{cm^{-3}}$)	$N_d(B)$ ($\mathrm{cm^{-3}}$)
1	3×10^{18}	49	1×10^{15}	1.5×10^{15}	3.4×10^{16}	5.2×10^{16}
2	5.0×10^{20}	52	1.8×10^{15}	2×10^{15}	5.5×10^{16}	1.2×10^{17}
3	1.3×10^{21}	55	2.8×10^{15}	4×10^{15}	9×10^{16}	1.5×10^{17}

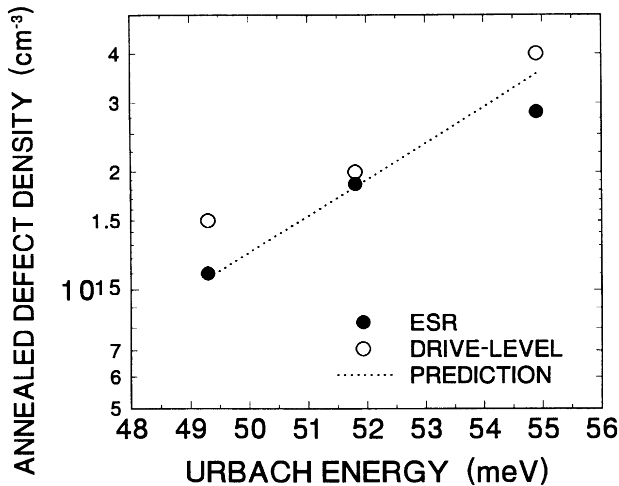

FIG. 8. Annealed deep-defect density as a function of the Urbach energy for the three samples of different carbon content shown in Fig. 7. The dashed line is the prediction of the spontaneous bond-breaking model of deep-defect formation.

mize disorder and strain by carefully optimizing the growth conditions. It is possible that a similar level of optimization may also be achieved for the addition of carbon to amorphous silicon. In that case these films would be expected to exhibit identical defect densities in the annealed state.

C. Metastability

In Sec. III we indicated that the samples containing higher concentrations of carbon impurities degraded to higher defect densities than the samples with lower carbon content. Specifically, after 3×10^4 s of high-intensity light soaking ($G>4.5\times10^{22}$ cm^{-3}), the sample with an impurity content of 2.6 at. % was found to degrade to a defect density roughly three times higher value than the samples with no intentional impurity content. This result is consistent with our earlier study of spatially modulated samples,[11] in which a sample with 1 at. % carbon exhibited a factor 2.2 higher defect density after light soaking compared to the most intrinsic sample. A similar result was obtained recently by Shimizu *et al.* who found the light-induced defect density to increase by a factor of 1.5 for samples with 0.8 at. % of carbon (compared to samples with a carbon content of 10^{17} cm^{-3}). All of these experimental results indicate that in the impurity range of 0.5–2 at. % there is an increase of approximately one defect for every 10 000 carbon atoms added. That is, although there is a definite enhancement of the light-induced degradation due to carbon impurities, the effect is rather small.

Recently much discussion has focused on the phenomenon of saturation, which is often observed in light-induced degradation experiments of *a*-Si:H.[30,31,2,32–34] In general, such saturation might arise either from a depletion of available defect precursor sites or from a balance between the creation and annealing of defects. For example, it has been suggested that the saturated density of light-induced defects depends on a fixed number of impurity sites, e.g., carbon atoms bonded to silicon atoms in the amorphous network.[3]

In the simplest such model, one might suppose that each carbon atom present in the network results in a metastable defect site after long-term light exposure. However, one can easily show that such a model cannot account for the experimental data available. Although some *a*-Si:H films grown in high-purity systems contain only about 10^{17} cm^{-3} of carbon atoms,[12] which approximately agrees with saturation defect densities of approximately 10^{17} cm^{-3}, most films have impurity levels of around 10^{18}–10^{19} cm^{-3}, with a saturation defect density of still only 10^{17} cm^{-3}.[2,13] Clearly, in such samples a much higher light-induced defect concentration should be found, in disagreement with experiments. Similarly, in the experiments described in this paper, the defect density increases only weakly with the concentration of carbon atoms incorporated.

On the other hand, such a weak dependence is consistent with recent studies that have demonstrated the role of light-induced annealing for the metastable defects.[32,35,36] This mechanism appears to be the dominant factor in determining the saturation value of the light-induced deep-defect density for experiments carried out at moderate to high generation rates at normal temperatures ($T\leq100$ °C). Such conditions apply to our current study. A quite general equation governing the rate of increase of deep defects with time, including the effects of light-induced annealing, was first proposed by Redfield and Bube.[37] However, for the case where thermal annealing effects can be ignored and where the density of precursor sites is much larger than the saturation values achieved, a simpler form has been suggested[32] which simply adds an annealing term to the electron-hole recombination term responsible for defect creation in the model originally given by Stutzmann, Jackson, and Tsai:[9]

$$\frac{dN_d}{dt}=\alpha\frac{G^2}{N_d^2}-\lambda N_d G \ , \tag{6}$$

where α and λ determine the rates of light-induced creation and annealing, respectively. Values for these parameters have been determined experimentally and vary somewhat between studies; however, values of $\gamma\equiv1/\alpha=0.01$–$0.1$ cm^3 s^{-1} and $\lambda=10^{-27}$–10^{-26} cm^3 are typical for our temperature range (310–330 K). Indeed, using the values $\gamma=0.21$ cm^3 s^{-1} and $\lambda=1.4\times10^{-27}$ cm^3 (assuming $G=4.5\times10^{22}$ cm^{-3} s^{-1}) gives an excellent fit to the DLCP data for our most intrinsic sample, as shown in Fig. 9 (including its saturation value of 5×10^{16} cm^{-3}).

The second term in Eq. (6) suggests that annealing occurs through a process that is initiated directly by an optical process at the defect site. In this case it is easily shown that the saturated defect density varies as

$$N_d^S=(\alpha G/\lambda)^{1/3} \ . \tag{7}$$

Alternatively, as some studies have suggested, the annealing process may be initiated by the capture of a photogenerated carrier.[38] This would lead to an annealing term of the form ΛG, instead of $\lambda N_d G$ as given in Eq. (6), and

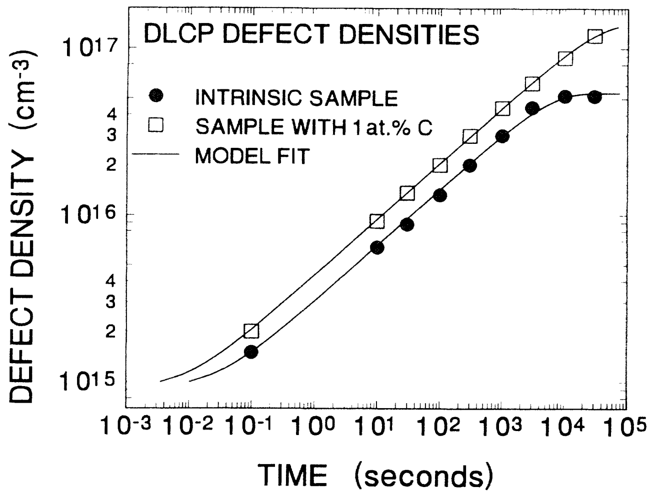

FIG. 9. Drive-level-determined deep-defect densities vs light exposure time: experiment and calculation. The calculation incorporates an electron-hole recombination defect creation term and a light-induced annealing term [Eq. (6)]. To account for the differences between the higher carbon sample compared to the intrinsic sample we must increase the coefficient for defect creation by a factor of 3, and decrease the coefficient of light-induced annealing by a factor of 6.

a square-root rather than a cube-root dependence in Eq. (7). Such a square-root dependence on generation rate may be more consistent with recent experiments.[34] In either case, however, the saturated defect densities are expected to exhibit a strongly sublinear dependence on α (and, in both cases, the presaturated densities would vary as $\alpha^{1/3}$).

If there exist definite precursor sites for light-induced defect creation, then the creation rate constant α will be proportional to the number of those sites and to the efficiency for the conversion of these sites into defects by the nonradiative recombination of electron-hole pairs. Thus the observed defect densities should approximately scale with the cube root of the number of precursor sites. This predicted dependence seems to provide a natural explanation for the relatively small changes in the defect densities that are observed upon adding carbon impurities.

On the other hand, if the level of carbon impurities really fixes the number of possible defect sites, then the number of defects could never exceed the number of carbon atoms in the films. This prediction may be contradicted by some experimental evidence showing that the density of metastable defects sometimes exceeds (although only marginally) the density of carbon atoms in low impurity films.[12,39,40] Thus, while carbon atoms may introduce extra precursor sites into the a-Si:H network, there probably already exists a considerable density of sites independent of these impurities.

Also, as we noted in Sec. III, the samples with higher levels of carbon impurities tended to saturate at later times than the more intrinsic samples. A similar result was suggested by Shimizu.[12] However, in the description given by Eq. (6) the time to reach saturation, t_S, is solely determined by the light-induced annealing term, that is[41]

$$t_S = \frac{2}{3\lambda G} . \tag{8}$$

For example, to account for the behavior of the sample with the 1 at. % carbon content requires not only that we increase the parameter α by a factor of 3 compared to the most intrinsic sample, to increase the overall larger densities of light-induced defects, but also that we decrease the parameter λ by a factor of 6. These parameters then provide a very good fit to the DLCP data for this sample, as shown in Fig. 9. (They also account quite well for the effects observed in the spatially modulated films at the 1 at. % carbon level of Ref. 11.) However, since λ should be independent of the number of defect sites, the concomitant changes in α and λ indicate that the effect of the carbon impurities is not a simple scaling up from the number of the precursor sites available in the more intrinsic samples.

Additional insight may be provided by an extension to the spontaneous bond breaking model of Stutzmann,[26] introduced in Sec. IV B to account for the stable defect densities. In this model, the creation of light-induced defects comes about because weak bonds located close to a demarcation energy E_{db} are shifted to an energy position beyond E_{db} and thus are transformed into dangling bonds. However, such newly created dangling bonds would quickly relax back into weak bonds unless they are stabilized by some means. Without specifying an exact mechanism we may assume that a potential barrier V_0 has to be overcome. If we assume that the energy available to create these dangling bonds is given by the tail-tail recombination energy E_r of electron-hole pairs, then the number of dangling bonds which can be converted will depend on the difference between this tail-tail recombination energy and the potential barrier for stabilization, e.g.,

$$\Delta E = \tfrac{1}{2}(E_r - V_0) , \tag{9}$$

where the factor $\frac{1}{2}$ would apply if the dangling bonds are created in pairs from each weak bond.[48] In this model the light-induced defect density ΔN_D is predicted to be

$$\Delta N_D = \int_{E_{\mathrm{db}}-\Delta E}^{E_{\mathrm{db}}} N_{\mathrm{tail}}(E)dE = N_D^0[\exp(\Delta E/E_u)-1] , \tag{10}$$

where N_D^0 is the stable deep-defect density given by Eq. (5). A good indication for the recombination energy E_r may be found by the energy distribution observed in photoluminescence experiments. These experiments generally show a linear relationship between the photoluminescence peak and the band gap of the samples;[42,43] however, the recombination energy will also depend on the carrier generation rate and on the measurement temperature. Noting that the band gap increases by 30–50 meV when 1 at. % carbon is incorporated in a-Si:H,[44] this description suggests that the light-induced defect density should roughly double with this level of carbon, as observed.

A correlation between light-induced degradation and

the optical-band gap of sample was observed several years ago[45] in a study that also investigated *a*-SiC:H. Although the authors of that study used only very weak light intensities and short degradation times, they found an essentially exponential dependence of the light-induced defect density on the band gap of the material. More recent studies[2,30,40,46] have confirmed such correlations between the saturated light-induced defect density and the band gap of the samples.

We note that the model described above also incorporates a density of precursor sites in the rate equations for light-induced degradation. But in contrast to models where the precursor sites are fixed by the number of impurities, the number of precursor sites in this case depends on changes in the mobility gap and the band-tail width as well as on the experimental conditions: the carrier generation rate and the degradation temperature.

V. CONCLUSION

We can summarize our key findings from this study as follows: First, we have found excellent agreement between the defect densities measured on samples with a Schottky-barrier configuration (drive-level capacitance, transient photocapacitance) and the defect densities measured on samples grown on quartz substrates (ESR). In particular, we have found good quantitative agreement between the ESR and the capacitance measurements for all light-soaked and annealed states of the samples. Therefore, since the capacitance measurements are sensitive to both charged defects and neutral defects, whereas the ESR measurements detects only neutral defects, we can conclude that the ratio of charged to neutral defects does not change significantly when the annealed samples are light soaked. We also can set an upper bound on the ratio of charged to neutral defects of about 2 to 1. This is an important result which contradicts predictions from some thermal equilibrium models.

Second, the annealed state defect density is increased when carbon is added to the material. At the 1 at. % carbon level the density of deep defects is increased by roughly a factor of 2. This increase is accompanied by an increase in width of the valence-band tail. The increase in defects can, therefore, be well accounted for in terms of a simple model in which the additional band-tail states lying beyond a certain demarcation energy are spontaneously converted into dangling bonds.

Third, the light-induced degradation of *a*-Si:H is also increased when carbon is added to the material. However, our results do not support predictions that each such impurity leads to an additional light-induced defect. Rather, at the 1 at. % level we observe only about one light-induced defect to be created per 10 000 carbon atoms added. Nontheless, although the effect is strongly sublinear in the concentration of carbon atoms, these results may be marginally compatible with the idea of impurity-related precursor sites for the light-induced defects. That is, for the case when light-induced annealing, rather than a limit to the number of precursor sites, is determining saturation, a strongly sublinear dependence on impurity levels is to be expected.

Fourth, the time to saturation of the light-induced defect density is significantly increased for the films with additional carbon (by at least a factor of 6). This observation cannot be explained simply in terms of an increase in precursor sites. This means that the light-induced degradation below about 0.1 at. % carbon has a qualitatively different character than that for films containing carbon at the 1 at. % level. This also implies an intrinsic susceptibility to light-induced effects that is independent of any carbon impurities.

Finally, the enhancement of the light-induced degradation that occurs when carbon is added to *a*-Si:H may be accounted for by the accompanying increase in band gap, even though such increases are quite small at the 1 at. % level. Within the spontaneous bond-breaking model an increase in band gap is expected to increase the energy available to stabilize the light-induced reconfiguration of bonds. Thus one would expect a larger number of weak silicon-silicon bonds to be converted into dangling bonds. This explanation is consistent with a number of other experiments which report a correlation between band gap and the saturated defect density of *a*-Si:H materials.

ACKNOWLEDGMENTS

We wish to thank Sally Asher for carrying out the SIMS analysis for the samples used in this study. This research was supported by NREL Subcontracts Nos. XG-1-10063-1 and XAN-4-13318-07.

---

*Present address: National Renewable Energy Laboratory, 1617 Cole Blvd., Golden, CO 80401.

†Present address: TEL America, 123 Brimbal Ave., Beverly, MA 01915.

[1]M. Nakata, S. Wagner, and T. M. Peterson, J. Non-Cryst. Solids **164-166**, 179 (1993).

[2]M. Isomura, X. Xu, and S. Wagner, Solar Cells **30**, 177 (1991).

[3]D. Redfield and R. Bube, Phys. Rev. Lett. **65**, 464 (1990).

[4]C. Magee and D. E. Carlson, Solar Cells **2**, 365 (1980).

[5]N. Nakamura, S. Tsuda, T. Takamaha, M. Nishikuni, K. Watanabe, M. Ohnishi, and Y. Kuwano, in *Optical Effect in Amorphous Semiconductors*, edited by P. C. Taylor and S. G. Bishop, AIP Conf. Proc. No. 120 (AIP, New York, 1984), p. 303.

[6]D. E. Carlson, A. Catalano, R. V. D'Aiello, C. R. Dickson, and R. S. Oswald, in *Optical Effect in Amorphous Semiconductors* (Ref. 6), p. 234.

[7]R. S. Crandall, D. E. Carlson, A. Catalano, and H. A. Weakliem, Appl. Phys. Lett. **44**, 200 (1984).

[8]R. S. Crandall, Phys. Rev. B **24**, 7457 (1981).

[9]M. Stutzmann, W. B. Jackson, and C. C. Tsai, Phys. Rev. B **32**, 23 (1985).

[10]A. Skumanich and N. M. Amer, Phys. Rev. B **37**, 8465 (1988).

[11]T. Unold and J. D. Cohen, J. Non-Cryst. Solids **114**, 603 (1989); Appl. Phys. Lett. **58**, 723 (1991).

[12]T. Shimizu, M. Matsumoto, M. Yoshita, M. Iwami, A. Mori-

moto, and M. Kumeda, J. Non-Cryst. Solids **137&138**, 391 (1991).

[13]M. Nakata, W. Wagner, C. W. Magee, T. M. Peterson, and H. R. Park, in *Amorphous Silicon Technology—1993,* edited by E. A. Scholl, M. J. Thompson, A. Malan, K. Tanaka, and P. G. LeComber, MRS Symposium Proceedings No. 297 (Materials Research Society, Pittsburgh, 1993), p. 369.

[14]For a preliminary report, see J. Hautala, T. Unold, and J. D. Cohen, in *Amorphous Silicon Technolgoy—1993* (Ref. 13), p. 375.

[15]D. V. Lang, J. D. Cohen, and J. P. Harbison, Phys. Rev. B **25**, 5285 (1982).

[16]SIMS analysis was carried out by Sally Asher, NREL.

[17]C. E. Michelson, A. V. Gelatos, and J. D. Cohen, Appl. Phys. Lett. **47**, 412 (1985).

[18]J. D. Cohen and A. V. Gelatos, in *Amorphous Silicon and Related Materials,* edited by H. Fritzsche (World Scientific, Singapore, 1989), p. 475.

[19]K. K. Mahadavi, K. Zellama, J. D. Cohen, and J. P. Harbison, Phys. Rev. B **35**, 7776 (1987).

[20]G. L. Miller, IEEE Trans. Electron Dev. **ED-19**, 1103 (1972).

[21]J. D. Cohen and D. V. Lang, Phys. Rev. B **25**, 5321 (1982).

[22]G. Schumm, W. B. Jackson, and R. A. Street, Phys. Rev. B **48**, 14 198 (1993).

[23]F. Zhong and J. David Cohen, Phys. Rev. Lett. **71**, 597 (1993).

[24]G. D. Cody, T. Tiedje, B. Abeles, B. Brooks, and Y. Goldstein, Phys. Rev. Lett. **47**, 1480 (1981).

[25]See, for example, M. B. Schubert, H. D. Mohring, E. Lotter, and G. H. Bauer, IEEE Trans. Electron Dev. **36**, 2863 (1989).

[26]M. Stutzmann, Philos. Mag. B **60**, 531 (1989).

[27]T. Unold, J. D. Cohen, and C. M. Fortmann, Appl. Phys. Lett. **64**, 1714 (1994).

[28]M. Stutzmann, R. A. Street, C. C. Tsai, J. B. Boyce, and S. E. Ready, J. Appl. Phys. **66**, 569 (1989).

[29]W. Paul, J. H. Chen, E. Z. Liu, A. E. Wetsel, and P. Wickboldt, J. Non-Cryst. Solids **164-166**, 1 (1993).

[30]H. R. Park, J. Z. Liu, and S. Wagner, Appl. Phys. Lett. **55**, 2658 (1989).

[31]D. Redfield and R. H. Bube, in *Amorphous Silicon Technology—1991,* edited by A. Madan, Y. Hamakawa, M. Thompson, P. C. Taylor, and P. G. LeComber, MRS Symposium Proceedings No. 219 (Material Research Society, Pittsburgh, 1991), p. 21.

[32]Z. Y. Wu, J. M. Siefert, and B. Equer, J. Non-Cryst. Solids **137&138**, 227 (1991).

[33]N. Hata, G. Ganguly, S. Wagner, and A. Matsuda, Appl. Phys. Lett. **61**, 1817 (1992).

[34]N. Hata, G. Ganguly, and A. Matsuda, in *Amorphous Silicon Technology—1993* (Ref. 14), p. 577.

[35]R. Meaudre and M. Meaudre, Phys. Rev. B **45**, 12 134 (1992).

[36]H. Gleskova, P. A. Morin, and S. Wagner, in *Amorphous Silicon Technology—1993* (Ref. 14), p. 589.

[37]R. H Bube and D. Redfield, J. Appl. Phys. **66**, 820 (1989).

[38]H. Gleskova, J. N. Bullock, and S. Wagner, J. Non-Cryst. Solids **164-166**, 183 (1993).

[39]M. Stutzmann, J. Nunnenkamp, M. S. Brandt, and S. Asano, Phys. Rev. Lett. **67**, 2347 (1991).

[40]A. Scholz and B. Schröder, in *Amorphous Silicon Materials and Solar Cells,* edited by B. L. Stafford, AIP Conf. Proc. No. 234 (AIP, New York, 1991), p. 179.

[41]Z.Y. Wu, J. M. Siefert, and B. Equer, J. Non-Cryst. Solids **137&138**, 227 (1991).

[42]R. A. Street, C. C. Tsai, M. Stutzmann, and J. Kakalios, Philos. Mag. B **56**, 289 (1987).

[43]W. Fuhs and F. Finger, J. Non-Cryst. Solids **114**, 387 (1989).

[44]H. Herremans, Ö. Öktü, W. Grevendonk, and G. J. Adriaenssens, J. Non-Cryst. Solids **137&138**, 855 (1991).

[45]A. Skumanich and N. M. Amer, Appl. Phys. Lett. **52**, 643 (1988).

[46]A. H. Mahan and M. Vanecek, in *Amorphous Silicon Materials and Solar Cells* (Ref. 40), p. 195.

[47]Inaccuracies of spin standards and other calibration procedures result in an overall scale factor uncertainty of at least 1.5 for both the ESR determined absolute spin densities and the DLCP determined absolute defect charge densities.

[48]T. Unold, in *Amorphous Silicon Technology—1994,* edited by E. A. Schiff, A. Madan, M. Hack, A. Matsuda, and M. Powell, MRS Symposia Proceedings No. 336 (Materials Research Society, Pittsburgh, 1994), pp. 387–292.